J Mater Sci (2007) 42:6222–6233
DOI 10.1007/s10853-006-1131-3

Theory of piezoresistivity for strain sensing in carbon fiber reinforced cement under flexure

Sirong Zhu · D. D. L. Chung

Received: 8 March 2006 / Accepted: 3 October 2006 / Published online: 20 April 2007

Abstract A theory is provided for piezoresistivity in carbon fiber reinforced cement (with and without embedded steel reinforcing bars) under flexure (three-point bending). The phenomenon, which involves the reversible increase of the tension surface electrical resistance and the reversible decrease of the compression surface electrical resistance upon flexure, allows strain sensing. The theory is based on the concept that the piezoresistivity is due to the slight pull-out of crack-bridging fibers during crack opening and the consequent increase in the contact electrtical resistivity of the fiber-matrix interface. This work is an extension of prior theory, which concerns the effect of uniaxial loading on the volume resistance. The extension requires modeling the surface resistance and its change under flexure. The theoretical results on the piezoresistivity, both with and without rebar, are in good agreement with prior experimental results. Differences between theoretical and experimental results are probably due to minor damage and rebar debonding during flexure.

Introduction

Cement reinforced with short carbon fibers has been shown to be able to sense its own strain [1–17] and damage [13–20] by DC electrical resistance measurement. The ability of a structural material to sense itself is known as self-sensing. Compared to the conventional method of attaining sensing by the use of embedded or attached sensors, self-sensing is advantageous in its low cost, high durability, large sensing volume and absence of mechanical property loss. In contrast, the use of embedded sensors tends to cause mechanical property loss to the structure.

The attributes in self-sensing can be strain (which relates to the stress), damage, temperature, etc. This paper is focused on the sensing of strain. Strain sensing is valuable for structural vibration control, weighing, traffic monitoring, border security, building facility management and other applications.

The self-sensing of strain can be attained by using piezoresistivity, i.e., the reversible effect of strain on the electrical resistance. The effectiveness of this method of self-sensing has been shown by experimental results obtained on carbon fiber reinforced cement during tension, compression and flexure [1–17]. Upon uniaxial compression, the volume resistance decreases (due to the slight push-in of crack-bridging fibers and the consequent decrease of the contact electrical resistivity of the fiber-cement interface); upon uniaxial tension, the volume resistance increases (due to the slight pull-out of crack-bridging fibers and the consequent decrease of the contact resistivity); upon flexure, the surface resistance on the tension side increases (as in the case of uniaxial tension), while that on the compression side decreases (as in the case of uniaxial compression) [2–7, 11, 17].

In the case of flexural loading, it has been shown that the piezoresistivity is enhanced by the presence of embedded steel reinforcing bars (rebars) [17]. Steel rebars are commonly used for reinforcing concrete, so the effect of the presence of steel rebars on the piezoresis-

Present Address:
S. Zhu
Department of Engineering Structures and Mechanics,
School of Science, Wuhan University of Technology,
Wuhan, Hubei 430070, China

D. D. L. Chung (✉)
Composite Materials Research Laboratory,
University at Buffalo State University of New York,
Buffalo, NY 14260-4400, USA
e-mail: ddlchung@buffalo.edu

tivity is relevant to practical implementation of the self-sensing.

Although there are numerous experimental results on the piezoresistivity of carbon fiber cement [2], theoretical work is scant [21]. Theoretical work is important for fundamental understanding of the piezoresistive phenomenon. In addition, a model of the phenomenon facilitates practical implementation. The prior theoretical work relates to a model of the piezoresistivity that is based on a mechanism involving slight fiber pull-out upon crack opening (push-in upon crack closing) and the consequent increase (decrease) in the contact electrical resistivity of the fiber-matrix interface [21]. This model has been applied to the cases of uniaxial tension and uniaxial compression, without steel reinforcing bars [21]. This paper extends this theory to the case of flexural loading, both with and without embedded steel reinforcing bars.

Basic theory of piezoresistivity in carbon fiber cement

This section reviews the basic theory of piezoresistivity in carbon fiber cement [21]. The theory concerns the effect of uniaxial loading on the volume resistance. A glossary of the abbreviations used in this paper is in Appendix 1.

The notion of fiber pull-out upon crack opening is illustrated in Fig. 1, which shows a cement element containing a carbon fiber under stress σ_x in the x direction. The angle between the fiber and σ_x is α. The extent of crack opening is exaggerated in Fig. 1 for the sake of illustration, as the crack opening is less than 1 μm, while the fiber length is about 5 mm [1]. Let the crack length perpendicular to the fiber in the plane of Fig. 1 be a.

Crack opening and closing occur only in the presence of tensile and compressive stresses respectively in the direction perpendicular to the plane of the crack. This normal stress σ_α, which is in the direction of the fiber, can be expressed as

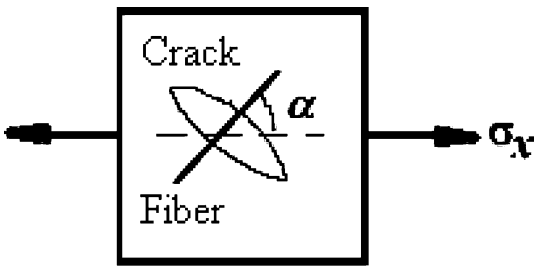

Fig. 1 A fiber bridging a crack in carbon fiber reinforced cement, with tensile stress σ_x applied at an angle α from the fiber axis. The extent of crack opening is exaggerated for the sake of illustration

$$\sigma_\alpha = \frac{\sigma_x}{2} + \frac{\sigma_x}{2}\cos 2\alpha \tag{1}$$

This normal stress gives rise to a force F_f acting in the direction of the fiber. This force is the pull-out force on the fiber. It is given by

$$F_f = at\sigma_\alpha = \tau A_c = \tau \cdot \pi d h_f, \tag{2}$$

where t is the thickness of the crack, τ is shear stress between the fiber and cement, A_c is contact area between the fiber and cement, d is the diameter of the fiber, and h_f is the length of the contact (interface) between the fiber and cement.

According to the equations of equilibrium,

$$\tau = \frac{at\sigma_\alpha}{\pi d h_f} \tag{3}$$

The electrical resistance of the specimen under study is contributed by conduction paths within the cement matrix surrounding a crack with the bridging fiber, in addition to the bridging fiber itself. The change in electrical resistance ΔR_s during loading is mainly contributed by the change in the contact resistance ΔR_c of the interface between fiber and cement, i.e.,

$$\Delta R_s = \Delta R_c \tag{4}$$

Single fiber pull-out testing [22] showed that the contact resistivity of the interface between carbon fiber and cement gradually increases with increasing shear stress prior to the abrupt increase when the shear stress reaches its maximum. For simplicity, we assume that the contact resistance increases linearly with the shear stress τ. Thus,

$$\Delta R_s = c\tau = c\frac{at}{\pi d h_f}\left(\frac{\sigma_x}{2} + \frac{\sigma_x}{2}\cos 2\alpha\right) \tag{5}$$

where c is a proportionality constant. Equation (5) shows that the change in resistance due to piezoresistivity depends on the fiber direction. This means that different fiber directions result in different levels of strain sensitivity.

Based on the data shown in Fig. 2 of Ref. 22, the curve of contact resistivity versus shear stress can be obtained. The slope k of this curve is

$$k = 0.1764 \times 10^5\,\Omega\,\mathrm{cm}^2/\mathrm{MPa} = 1.764 \times 10^{-6}\,\Omega\,\mathrm{m}^2/\mathrm{Pa} \tag{6}$$

Since $\Delta R_s = \Delta R_c = \Delta(\rho_c/A_c) = \Delta(\rho_c/\pi\ d\ h_f) = c\tau$,

$$c = k/A_c = k/\pi d h_f = 1.764 \times 10^{-6}/\pi d h_f (\Omega\,\mathrm{m}^2/\mathrm{Pa}) \tag{7}$$

Using Eqs. (3) and (7),

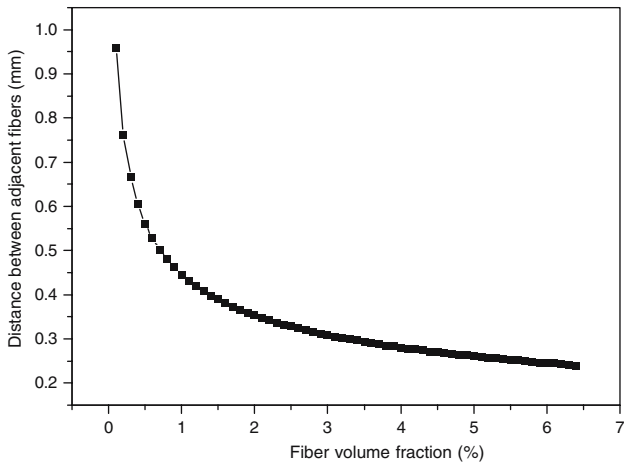

Fig. 2 Variation of the distance between the ends of adjacent fibers with the fiber volume fraction

$$\Delta R_s = \frac{1.764 \times 10^{-6} at}{2\left(\pi d h_f\right)^2} \sigma_x (1 + \cos 2\alpha) \tag{8}$$

The carbon fibers in cement are distributed randomly. Although there is a slight tendency for the fibers to lie down in the horizontal plane of the specimen during setting and curing, the degree of preferred orientation is slight and is negligible when the specimen is more than 25 mm high in the vertical direction during setting and curing [11]. A high degree of fiber dispersion is attained by the use of silica fume and methylcellulose as admixtures and by ozone treatment of the fiber prior to using the fiber [23]; these fiber dispersion techniques were indeed used in the experimental work [17] that provided the experimental results employed in this paper for comparison between theoretical and experimental results. Thus, it can be considered that, on the average, every fiber has the same contribution to the piezoresistive effect. Therefore, ΔR_s can be averaged from $\alpha = 0°$ to $\alpha = 90°$, thereby removing the dependence on α. Integrating both sides of Eq. (5) with respect to α and taking the average value over α, we have

$$\begin{aligned} \Delta R_s &= \frac{2}{\pi} \int_0^{\frac{\pi}{2}} c \frac{at}{\pi d h_f} \left(\frac{\sigma_x}{2} + \frac{\sigma_x}{2} \cos 2\alpha \right) d\alpha \\ &= \frac{cat}{2\pi d h_f} \sigma_x \\ &= \frac{1.764 \times 10^{-6} at}{2\pi^2 d^2 h_f^2} \sigma_x \end{aligned} \tag{9}$$

Distribution of carbon fibers in cement

Different fiber volume fractions result in different numbers of fibers in a carbon fiber cement element. Let the fiber volume fraction be C_f, the volume of a carbon fiber cement specimen be V, and the length of a carbon fiber be l_f. Then the volume of all the fibers in the specimen is

$$V_f = C_f V \tag{10}$$

and the number of fibers is

$$N = \frac{V_f}{\frac{\pi}{4} d^2 l_f} \tag{11}$$

Under the condition of uniform fiber distribution, it can be considered that the ends of all fibers (one end of every fiber being considered as the position of the fiber) are uniformly distributed, with every fiber end occupying a small cube of volume V_o:

$$V_o = \frac{V}{N} = \frac{\frac{\pi}{4} d^2 l_f}{C_f} \tag{12}$$

The distance S between the ends of two adjacent fibers is the length of an edge of the small cube, that is

$$S = \sqrt[3]{V_o} = \sqrt[3]{\frac{\frac{\pi}{4} d^2 l_f}{C_f}} \tag{13}$$

Figure 2 shows the dependence of the distance (a) between the ends of adjacent fibers on the fiber volume fraction, as obtained by using Eq. (13), with $d = 15$ μm and $l_f = 5$ mm. When $C_f = 0.48\%$, $S = 0.57$ mm.

Modeling the electrical resistance

The modeling of the electrical resistance is necessary for modeling the piezoresistive behavior, since the resistance is the quantity measured in the piezoresistivity experiment. Two types of resistance are measured during flexure, namely the surface resistance and the through-thickness resistance [17]. Section 'Modeling the surface electrical resistance' provides a model for the surface resistance; Sect. 'Modeling the through-thickness resistance' provides a model for the through-thickness resistance; Sect. 'Comparison of measured and calculated resistance values' provides a comparison of the calculated and measured resistance values.

Modeling the surface electrical resistance

The surface electrical resistance is the resistance measured by using electrical contacts that are on one surface of a specimen, as illustrated in Fig. 3, where the contacts are on the tension surface (for measuring the tension surface

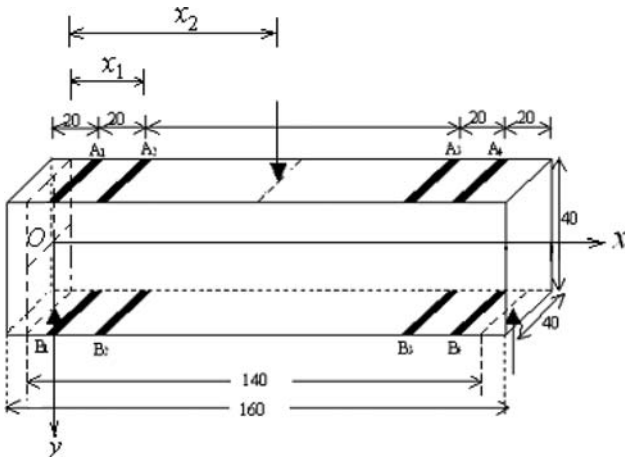

Fig. 3 Specimen configuration for flexural testing by three-point bending. The three points are shown by arrows. A_1, A_2, A_3 and A_4 are electrical contacts on the compression surface, whereas B_1, B_2, B_3 and B_4 are electrical contacts on the tension surface. All dimensions are in mm. From Ref. [17]

resistance) and on the compression surface (for measuring the compression surface resistance) of a specimen under flexure. The surface current contacts allow the current to be injected from one surface, rather than being injected uniformly throughout the cross section of the specimen. The surface voltage contacts allow the voltage to be measured on the surface. Thus, the surface resistance, as obtained by dividing the voltage between the surface voltage contacts by the current injected by the surface current contacts, is to be distinguished by the volume resistance, which is ideally measured by using current contacts that allow uniform current injection throughout the cross section. Due to the assumed uniformity of the current density in the cross section of the specimen in the case of volume resistance measurement, the volume resistance is simply related to the volume electrical resistivity of the specimen. However, due to the non-uniformity in the current density in the case of surface resistance measurement, the surface resistance is not simply related to the volume resistivity.

The utilization of the piezoresistivity of carbon fiber reinforced cement under flexure mainly involves measurement of the surface resistance. This section provides a model for the surface resistance. This model is used in Sect. 'Extension of piezoresistivity theory to flexure', which provides a model for the piezoresistivity under flexure.

The surface electrical resistance is measured using the surface electrical contacts shown in Fig. 3, where a carbon fiber cement beam is under flexure (three-point bending). The compression surface resistance was measured by using A_1 and A_4 as current contacts and A_2 and A_3 as voltage contacts. The tension surface resistance was measured by using B_1 and B_4 as current contacts and B_2 and B_3 as voltage contacts. The through-thickness resistance was measured by using A_1 and B_1 as current contacts and A_2 and B_2 as voltage contacts.

Because the stress is different at different points along the thickness of the beam, the resistance change varies among these points. Hence, the beam is divided into n layers which are stacked in the thickness direction, such that each layer is of thickness equal to the distance S between the ends of adjacent fibers (Eq. (13)). Hence,

$$n = \frac{h}{S} \tag{14}$$

In order to calculate the total change in resistance ΔR, we use an equivalent electrical circuit to describe the beam, as shown in Fig. 4. In each layer there are two resistances ($R_L(i)$ and $R_T(i)$) which correspond to two directions of electrical conduction, namely the longitudinal direction (x-axis) and the through-thickness direction (y-axis). Both resistances contribute to the surface resistance (whether at the tension or compression surface), which is the quantity measured.

In the equivalent circuit of Fig. 4, $R_L(i)$ is the longitudinal resistance of the ith layer. It is associated with an element of length L_V (the distance between the two inner contacts, A_2 and A_3, shown in Fig. 3), thickness S and width b. Hence,

$$R_L(i) = \frac{\rho L_V}{bS} \tag{15}$$

where ρ is the volume electrical resistivity.

In the circuit of Fig. 4, $R_T(i)$ is the through-thickness resistance of the ith layer. The element associated with $R_T(i)$ is taken to be of length S in the through-thickness

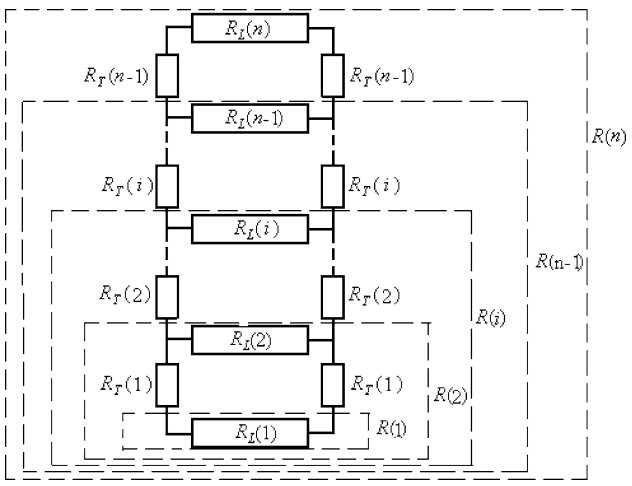

Fig. 4 Equivalent electrical circuit used for calculating the surface resistance

direction and width S in the longitudinal direction, since the current path actually bows into the specimen from the surface and the thickness of the bowed path is considered to be S. Hence,

$$R_T(i) = \frac{\rho S}{bS} \tag{16}$$

To be exact, L_V in Eq. (15) should be reduced by $2S$, in order to avoid counting the same element as contributing to both $R_L(i)$ and $R_T(i)$. However, since $2S$ is small compared to L_V, this reduction is not performed in this work.

The top surface resistance $R(n)$, i.e., the resistance measured between the two terminals of resistor $R_L(n)$, is calculated by considering this surface resistance to be $R_L(n)$ in parallel with the sum of $R_T(n–1)$, $R_L(n–1)$ and $R_T(n–1)$ (i.e., these three resistances in series in Fig. 4). In general, the resistance $R(i)$ between the two terminals of $R_L(i)$ is obtained by considering $R_L(i)$ in parallel with the sum of $R_T(i–1)$, $R_L(i–1)$ and $R_T(i–1)$. In other words,

$$R(1) = R_L(1) \tag{17}$$

$$R(i) = \frac{(2R_T(i-1) + R(i-1))R_L(i)}{R_L(i) + 2R_T(i-1) + R(i-1)} (i = 1, \ldots.., n) \tag{18}$$

and

$$R(n) = \frac{(2R_T(n-1) + R(n-1))R_L(n)}{R_L(n) + 2R_T(n-1) + R(n-1)} \tag{19}$$

Although Eq. (19) gives the resistance measured between two points on the surface (i.e., A_2 and A_3 in Fig. 3), it can be used to calculate the resistance measured between the corresponding two points on any of the layers in Fig. 5.

Modeling the through-thickness resistance

The through-thickness resistance in this work refers to the resistance measured between A_2 and B_2 in Fig. 3. This resistance is one of the measured quantities [17], so the modeling of this resistance is provided in this section.

The model of the surface resistance, as presented in Sect. 'Modeling the surface electrical resistance', involves layers in the longitudinal direction for the purpose of calculating the longitudinal surface resistance $R(n)$ based on the values of R_T and R_L for the various layers. This model can be modified by having the layers perpendicular to the longitudinal direction for the purpose of calculating the through-thickness resistance, as illustrated in Fig. 6. In the modified model, the electrical circuit model of Fig. 4 is modified so that R_L is replaced by R_T and R_L is replaced by R_L. Hence, the through-thickness resistance is given by the following equation, which is obtained by modifying Eq. (19) as applied to the resistance between two points on an interior layer.

$$R(n) = \frac{(2R_L(n-1) + R(n-1))R_T(n)}{R_T(n) + 2R_L(n-1) + R(n-1)} \tag{20}$$

Comparison of measured and calculated resistance values

Using the model of Sect. 'Modeling the surface electrical resistance', we calculated the surface resistance.

A more robust model may include the shear stress in Eq. (1). The present model is accurate in regions with large moment and small shear, though the experimental measurements [17] were conducted over almost the entire length of the beam.

Calculation of the surface resistance was based on Eq. (19) and a value of the volume resistivity that was obtained either from the use of Eq. (19) and the measured surface resistance [17] or from the use of Eq. (20) and the measured through-thickness resistance [17]. Calculation of the through-thickness resistance was based on Eq. (20) and a value of the volume resistivity that was obtained either from the use of Eq. (19) and the measured surface

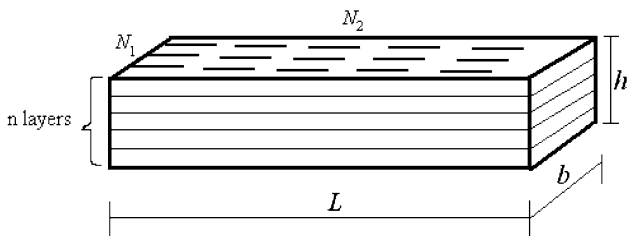

Fig. 5 Schematic illustration of the layers in the plane of the beam in the model for calculating the surface resistance. The fibers in the top layer are schematically illustrated by using short lines in the longitudinal direction

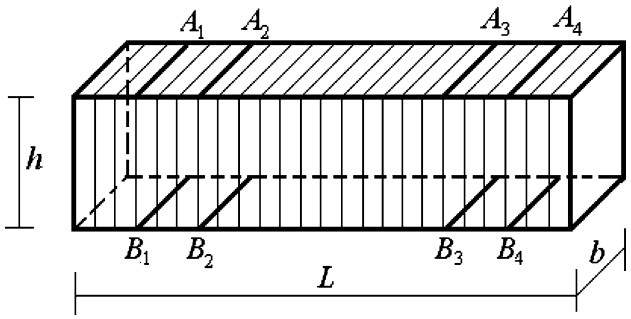

Fig. 6 Schematic illustration of the layers in the plane perpendicular to the longitudinal direction in the model for calculating the through-thickness resistance

resistance [17] or from the use of Eq. (20) and the measured through-thickness resistance [17]. Reasonably good agreement is found between the calculated and measured values for both the surface resistance and the through-thickness resistance, as shown in Table 1.

Based on the measured surface resistance and the surface resistance model, the volume resistivity is found to be 1.84×10^5 Ω cm. (Table 1). This value is high compared to the separately measured volume resistivity of 1.5×10^4 Ω cm [11]. This discrepancy is probably due to the presence of a surface layer which affects the surface resistance measurement. This layer may be different from the interior of the specimen in terms of the preferred orientation and concentration of the fibers, thus resulting in greater difficulty of current penetration. Such a surface layer is expected to affect strongly the measured surface resistance, though it has relatively little effect on the measured volume resistivity.

Extension of piezoresistivity theory to flexure

This section provides an extension of the piezoresistivity theory described in Sect. 'Basic theory of piezoresistivity in carbon fiber cement' for carbon fiber cement under uniaxial loading to a carbon fiber cement beam under flexure (three-point bending). Under flexure, the moment and normal stress are respectively

$$M = \frac{P}{2}x$$
$$\sigma_x = \frac{My}{I_z} = \frac{Pxy}{2I_z}, \tag{21}$$

Table 1 Measured and calculated values of the resistance

Resistance type	Measured resistance (10^5 Ω)	Calculated resistance (10^5 Ω)	
Surface	7.2	7.2[a]	6.2[c]
Through-thickness	4.2	4.8[b]	4.2[d]

[a] Based on Eq. (19) and volume resistivity of 1.84×10^5 Ω cm, which is obtained from the use of Eq. (19) and the measured surface resistance value

[b] Based on Eq. (20) and volume resistivity of 1.84×10^5 Ω cm, which is obtained from the use of Eq. (19) and the measured surface resistance value

[c] Based on Eq. (19) and volume resistivity of 1.57×10^5 Ω cm, which is obtained from the use of Eq. (20) and the measured through-thickness resistance value

[d] Based on Eq. (20) and volume resistivity of 1.57×10^5 Ω cm, which is obtained from the use of Eq. (20) and the measured through-thickness resistance value

where x is the position along the neutral axis of the beam, y is the distance from the neutral axis (Fig. 3), P is the force, and I_z is the moment of inertia of the cross section of the beam.

Combining Eqs. (9) and (21) gives

$$\Delta R_s = \frac{catPxy}{4\pi dh_f I_z} = \frac{1.764 \times 10^{-6} atPxy}{4\pi^2 d^2 h_f^2 I_z} \tag{22}$$

Equation (22) shows the change of resistance of a cement specimen with a single carbon fiber under flexure. Actually, there are a large number of carbon fibers in a cement specimen and they are both in series and in parallel. Figure 5 illustrates the fiber distribution, where all fibers are considered in the same direction (as justified by the angular averaging in Eq. (9) and the consequent removal of the angular dependence), such as the x direction in Fig. 3. There are N_1 fibers that are in parallel along the edge of length b, and there are N_2 fibers that are in series along the edge of length L, as shown in Fig. 5. From Equation (22), the change of resistance depends on the location (i.e., the coordinates x and y) of the fiber.

Under flexure, the top part of the beam is compressed and both resistances in this part decrease, whereas the bottom part of the beam is tensioned and both resistances in this part increase. Although the longitudinal resistance is affected by flexure more than the through-thickness resistance, both resistances are affected in the same way. This notion is based on prior experimental results for carbon fiber cement under uniaxial compression [5] and uniaxial tension [6]. Under uniaxial compression, both the longitudinal and transverse resistances increase; the transverse resistance increases in spite of the Poisson effect, which causes slight transverse shrinkage. Under uniaxial compression, both the longitudinal and transverse resistances decrease; the transverse resistance decreases in spite of the Poisson effect, which causes slight transverse elongation.

N_1 and N_2 are given by

$$N_1 = \frac{b}{S} \tag{23}$$

and

$$N_2 = \frac{N}{nN_1}, \tag{24}$$

Since the N_1 fibers in one row of fibers in a layer (Fig. 5) are electrically in parallel in the longitudinal direction (x-axis), they together give a resistance change ΔR_1 that is equal to $1/N_1$ of that given by a single fiber. Hence,

$$\Delta R_1(i) = \frac{\Delta R_s}{N_1} = \frac{\frac{1.764\times10^{-6} atPxy_i}{4\pi^2 d^2 h_f^2 I_z}}{N_1} \tag{25}$$

Equation (25) means that ΔR_1 is a function of x and y. Thus, it can be written as ΔR_1 (x,y_i).

One layer consists of N_2 groups of N_1 fibers that are electrically in series along the x-axis. Hence, the resistance change due to the ith layer is

$$\Delta R_L(i) = \sum_{N_2} \Delta R_1(x, y_i) \tag{26}$$

In one layer, y is a constant. Hence, Eq. (26) shows that ΔR_1 is a linear function of x. By symmetry, the average value of ΔR_1 (x,y) can be approximated as that at $x = \frac{x_1+x_2}{2}$, where x_1 and x_2 are as defined in Fig. 3. Hence,

$$\begin{aligned}\Delta R_L(i) &= \sum_{N_2} \Delta R_1(x, y_i) = N_2 \frac{1.764\times10^{-6} atPxy_i}{4N_1\pi^2 d^2 h_f^2 I_z} \\ &= \frac{1.764\times10^{-6} N_2}{8N_1\pi^2 d^2 h_f^2 I_z} atPy_i(x_1 + x_2)\end{aligned} \tag{27}$$

Based on prior experimental results under uniaxial tension and uniaxial compression, the magnitude of the transverse gage factor (i.e., the fractional change in resistance in the transverse direction per unit strain in the transverse direction) is roughly the same as that of the longitudinal direction [5, 6]. Since the through-thickness strain is related to the longitudinal strain by the Poisson ratio v,

$$\Delta R_T(i) = v\frac{R_T(i)}{R_L(i)}\Delta R_L(i) \tag{28}$$

In flexural experiments, the midspan deflection is a quantity that is usually measured. Therefore, ΔR in Eq. (30) and (31) needs to be expressed as a function of the midspan deflection f. For a beam under three-point bending,

$$f = \frac{PL^3}{48EI_z} \tag{29}$$

Combining Eqs. (27), (28) and (29) gives

$$\Delta R_L(i) = \frac{1.764\times10^{-6}\times48EfN_2}{8N_1\pi^2 d^2 h_f^2 L^3} aty_i(x_1 + x_2) \tag{30}$$

$$\Delta R_T(i) = v\frac{R_T(i)}{R_L(i)}\frac{1.764\times10^{-6}\times48EfN_2}{8N_1\pi^2 d^2 h_f^2 L^3} aty_i(x_1 + x_2) \tag{31}$$

Equations (30) and (31) give the change in the change in the resistance of the ith layer due to piezoresistivity. The parameter at in Eqs. (30) and (31) describes the area of a crack. For cement-based materials, crack areas can range from square micrometer to square millimeter [24].

Upon flexure, all the resistances in Fig. 5 change. Let $R_L(i)$, $R_T(i)$ and $R(i)$ change to $R'_L(i)$, $R'_T(i)$ and $R'(i)$ respectively. In other words,

$$R'_L(i) = R_L(i) + \Delta R_L(i) \quad (i = 1, \ldots\ldots, n) \tag{32}$$

$$R'_T(i) = R_T(i) + \Delta R_T(i) \quad (i = 1, \ldots\ldots, n-1) \tag{33}$$

$$R'(i) = \frac{(2R'_T(i-1) + R'(i-1))R'_L(i)}{R'_L(i) + 2R'_T(i-1) + R'(i-1)} \quad (i = 1, \ldots\ldots, n) \tag{34}$$

and

$$R'(n) = \frac{(2R'_T(n-1) + R'(n-1))R'_L(n)}{R'_L(n) + 2R'_T(n-1) + R'(n-1)} \tag{35}$$

Hence, the total change in the top surface resistance is given by

$$\Delta R = R'(n) - R(n) \tag{36}$$

and the fractional change of resistance is

$$\frac{\Delta R}{R(n)} = \frac{R'(n) - R(n)}{R(n)} \tag{37}$$

Comparison of measured and calculated piezoresistive behavior

The piezoresistivity under flexure is described by the model in Sect. 'Extension of piezoresistivity theory to flexure'. This section provides a comparison of the calculated and measured [17] piezoresistive behavior, in order to test the effectiveness of the model. Two cases are considered in this section, namely the case without steel rebar (Sect. 'Carbon fiber cement without steel rebar') and the case with embedded steel rebars (Sect. 'Carbon fiber cement with embedded steel rebars').

Practical implementation of the flexural strain sensing can involve measurement of the surface resistance at either the tension side or the compression side. The choice depends on the configuration of the particular structure.

Carbon fiber cement without steel rebar

The prior experimental work [17], with the specimen beam as shown in Fig. 3, involves $d = 15$ μm, $h_f = 5$ mm (since the nominal fiber length is 5 mm), C_f = 0.48 vol.%

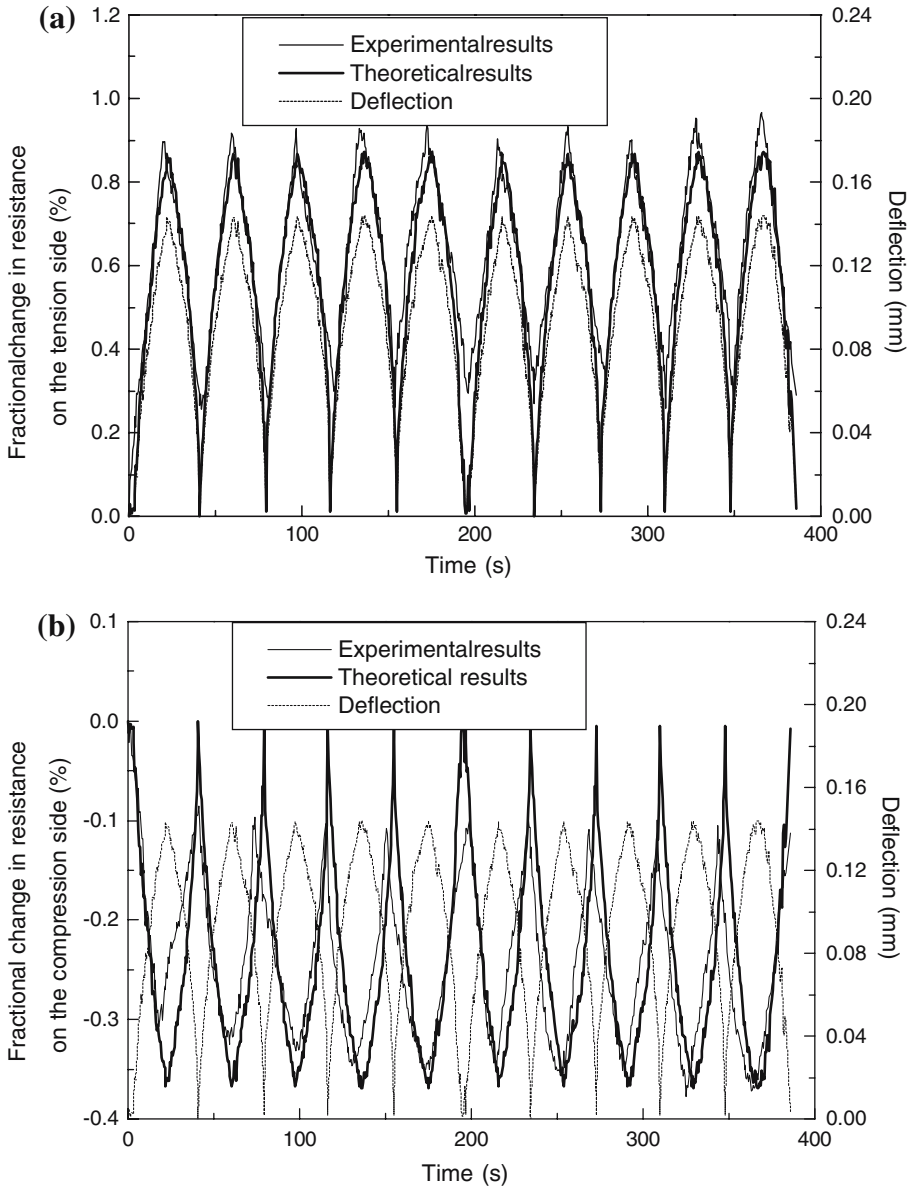

Fig. 7 Comparison of the calculated and measured curves for the change in surface resistance upon repeated flexure for carbon fiber cement beam without rebar. (**a**) The tension side. (**b**) The compression side. Measured results are from Ref. [17]

(corresponding to fibers in the amount of 0.5% by mass of cement), E = 13 GPa [5, 6], x_1 = 30 mm, and x_2 = 70 mm. Assume that $at = 1.9 \times 10^{-10}$ m^2 for the tension side; $at = 8.5 \times 10^{-11}$ m^2 for the compression side. It is reasonable that, at the same deflection, cracks are much larger at the tension side than the compression side, and then carbon fiber cement is more sensitive to tensile stress. This is because cement is much weaker under tension than compression.

The calculated and measured values of the change in surface resistance during repeated flexure at a maximum deflection f of 0.143 mm (experimental value of f in the first cycle) are compared in Fig. 7(a) and (b) for the tension and compression surfaces respectively. Comparison of the calculated and measured curves shows good agreement between them, although the partial irreversibility of the measured resistance change after the first cycle causes some difference after the first cycle. For the tension side, the measured resistance is irreversibly increased after the first cycle; for the compression side, the measured resistance is irreversibly decreased after the first cycle. These irreversible effects are attributed to minor damage, which is known to cause the resistivity to increase irreversibly [18, 20, 21, 24].

Under uniaxial tension, the volume resistance increases upon loading, such that there is slight partial irreversibility in the resistance increase after unloading [6]. The irreversible increase is due to minor damage. This irreversible increase is consistent with the irreversible increase in the tension surface resistance during flexural loading [17].

Under uniaxial compression, the volume resistance decreases upon loading, such that the resistance is irreversibly

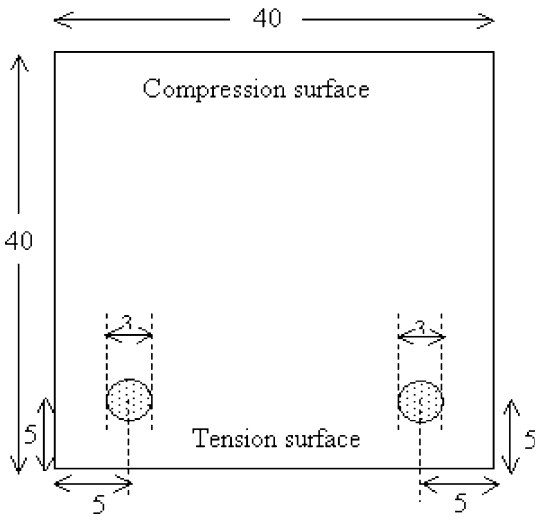

Fig. 8 Cross-sectional illustration of a carbon fiber cement beam containing two steel rebars (dotted regions). All dimensions are in mm. From Ref. [17]

increased after unloading [5]. This irreversible increase is not consistent with the irreversible decrease in the compression surface resistance during flexural loading [17]. This inconsistency for the compression case suggests that the type of damage under uniaxial compression is not the same as that at the compression surface during flexure. The stress is highest at the midspan position in case of flexure, thus causing the damage to be concentrated at the midspan position. On the other hand, the stress is uniformly distributed in case of uniaxial compression, so that the damage is spread out. Damage that is associated with an irreversible resistance decrease, as in the case of flexure, may be due to excessive crack closing, i.e., crack squeezing; this type of damage is relatively severe. Damage that is associated with an irreversible resistance increase, as in the case of uniaxial compression, may be due to an irreversible degradation of the fiber-matrix interface; this type of damage is relatively subtle.

Carbon fiber cement with embedded steel rebars

The carbon fiber cement beams with embedded steel rebars, as illustrated in Fig. 8 in terms of the cross-sectional view, are identical in dimensions to those without steel rebar. The rebars are near the tension surface. Prior to any loading, the tension surface resistance is slightly smaller in the presence of rebars, as shown by comparing the R_0 value indicated in Fig. 7(a) (case without rebar) and Fig. 9(a) (case with rebars). This means that the tension surface current penetrates slightly into the steel rebars. The beams with and without rebars were tested at essentially the same maximum deflection [17].

Comparison of the experimentally obtained stress-deflection relationship for the cases with and without rebars, along with E = 13 GPa [5, 6] for the case without rebar, gives E = 14 GPa for the case with rebars. Figure 9 shows comparison of the theoretical and experimental results for carbon fiber cement beams with embedded steel rebars. For the tension side, $at = 1.9 \times 10^{-10}$ m^2;for the compression side $at = 8.5 \times 10^{-11}$ m^2. These values are the same the corresponding values for the case without rebars (Sect. 'Carbon fiber cement without steel rebar'). The cracks on the tension sides are larger than those on the compression side, as in the case without rebar.

The agreement between the calculated and measured curves in Fig. 8 is not as good as that for the case without rebar (Fig. 7). In Fig. 9, the calculated change in resistance at the maximum deflection of each cycle is less than the measured change in resistance for both tension and compression surfaces. This difference between calculated and measured curves is probably due to the partial debonding between rebar and cement during flexure increasing the contact electrical resistivity of the interface between rebar and cement [25–27], thereby decreasing the extent of penetration of the tension surface current into the rebar and hence increasing the current density at the tension surface. The increase in surface current density causes the measured surface resistance to increase. This effect adds to the piezoresistive effect of the carbon fiber cement, thus causing the measured resistance increase during flexural loading to be larger than the theoretical value. The theory does not take into account the effect of debonding at the interface between rebar and cement.

The irreversible increase in the tension surface resistance and the irreversible decrease in the compression surface resistance after the first cycle (as in the case without rebar) cause additional difference between the theoretical and experimental curves, as shown in Fig. 9. The irreversible effect on the compression side is more severe than the case without rebar. This is attributed to the low local stiffness of the compression side compared to the tension side (due to the proximity of the rebars to the tension surface) and high overall stiffness when rebars are present. As a consequence of these stiffness issues, the extent of damage on the compression surface for the case with rebars is larger than that for the case without rebar, with both cases at the same deflection.

The presence of steel rebars decreases the number (N_1) of carbon fibers in parallel (Fig. 5), thereby increasing ΔR. The theoretical curves in Fig. 9 do not take into account this effect of the rebars. However, calculation shows that this effect is negligible, due to the small diameter of the rebars used.

Comparison of results for cases with and without rebars

Comparison of Fig. 7 and 9 shows that the change in electrical resistance upon flexure at the same deflection is

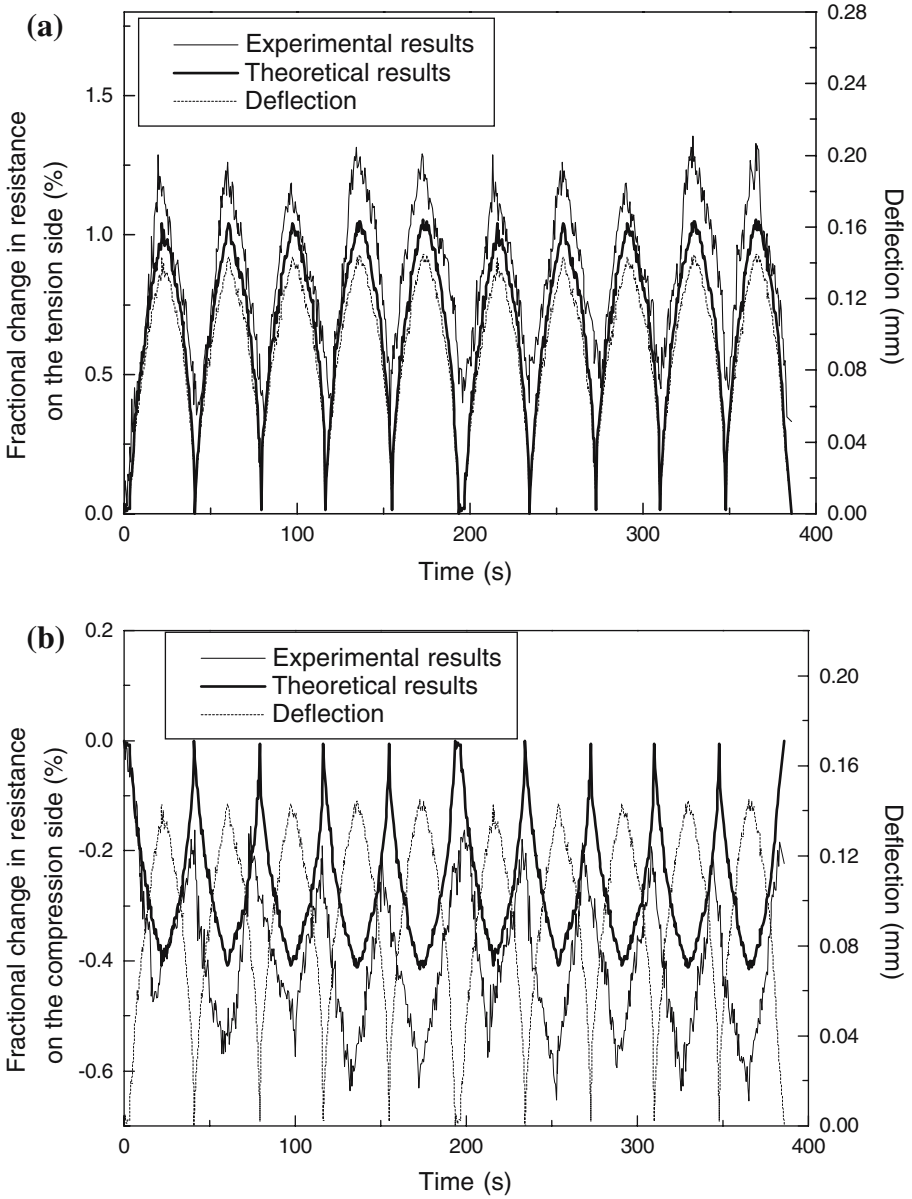

Fig. 9 Comparison of the calculated and measured curves for the change in surface resistance for carbon fiber cement beam with embedded steel rebars. (**a**) The tension side. (**b**) The compression side. Measured results are from Ref. [17]

higher in the presence of embedded steel rebars. This is because the nominal elastic modulus of the beam is higher in the presence of rebars. It is well-known that the elastic modulus of steel is much higher than that of cement. Equations (24) and (25) indicate that the change in resistance increases with the elastic modulus E for the same strain (i.e., the same midspan deflection f). In the elastic range, Hooke's Law is satisfied, so that, for the same strain, a higher modulus gives a higher stress. Thus, the piezoresistive effect is enhanced by the presence of steel rebars.

Conclusion

A model for the piezoresistivity in carbon fiber reinforced cement under flexure is provided. This model explains the effect of flexure on the electrical resistance of the tension and compression surfaces of a beam, for both the cases with and without embedded steel rebars near the tension surface. The model is based on the notion that the piezoresistivity is due to the slight pull-out of crack-bridging fibers during crack opening and the consequent increase in the contact electrical resistance of the fiber-matrix interface. Good agreement has been attained between calculated and measured results, though differences occur, probably due to minor damage and rebar debonding.

Acknowledgements This work was supported in part by the Key Project of National Natural Science Foundation of China under grant No. 50238040. The authors appreciate technical discussion with Dr. Sihai Wen of University at Buffalo, State University of New York.

Appendix

Table 2 Appendix: Glossary of abbreviations

σ_x	Normal stress in the x direction
σ_α	Normal stress in the direction of angle α
α	Angle between the x axis and the stress direction
F_f	Force acting in the direction of the fiber
a	Crack length
t	Crack thickness
τ	Shear stress between the fiber and cement
A_c	Contact area between the fiber and cement
d	Diameter of a carbon fiber
h_f	Length of the contact (interface) between a fiber and cement
ΔR_s	Change in electrical resistance during loading
ΔR_c	Change in the contact resistance of the interface between fiber and cement
k	Slope of curve of contact resistivity versus shear stress
ρ_c	Contact electrical resistivity between a fiber and cement
A_c	Contact area between a fiber and the cement matrix
c	Proportionality constant that relates the resistance change and the shear stress change
C_f	Carbon fiber volume fraction
V	Volume of a carbon fiber cement specimen
l_f	Length of a carbon fiber
V_f	Volume of all the fibers
N	Total number of fibers
V_o	Volume of a cube containing a fiber end
S	Distance between the ends of two adjacent fibers, thickness of one layer
M	Moment of a cross section of a beam
P	Force acting on a beam
x	Position along the neutral axis of a beam and the axial direction of a beam
y	Distance from the neutral axis in the through-thickness direction of the beam
I_z	Moment of inertia of the cross section of a beam
b	Width of a beam
h	Height of a beam
L	Span
N_1	Number of fibers that are in parallel along the edge of length b
N_2	Number of fibers that are in series along the length L of the beam
n	Number of layers in a beam
i	The ith layer
ΔR	Total change in resistance measured at the top surface
$R_L(i)$	Resistance in the longitudinal direction (x-axis) of the ith layer
$R_T(i)$	Resistance in the through-thickness direction (y-axis) of the ith layer
ΔR_1(i)	Change of resistance of the ith layer due to N_1 fibers in parallel
ΔR_L(i)	Change of $R_L(i)$
ΔR_T(i)	Change of $R_T(i)$
x_1	x coordinate of the electrical contact A_2 in Fig. 3
x_2	x coordinate of the mid-point of the beam in Fig. 3
E	Elastic modulus of the beam material
y_i	Distance between the ith layer and the neutral axis
f	Deflection of the beam at midspan
v	Poisson ratio
ρ	Volume electrical resistivity of carbon fiber reinforced cement

Table 2 continued

L_V	Distance between the two inner contacts, A_2 and A_3, in Fig. 3
$R(i)$	Resistance between the two terminals of $R_L(i)$
$R'_L(i)$	Changed value of $R_L(i)$ upon flexure
$R'_T(i)$	Changed value of $R_T(i)$ upon flexure
$R'(i)$	Changed value of $R(i)$ upon flexure

References

1. Chen P-W, Chung DDL (1996) Compos Part B – Eng 27B:11
2. Chung DDL (2002) J Intel Mat Syst Str 13(9):599
3. Wen S, Chung DDL (2003) Adv Cem Res 15(3):119
4. Chung DDL (2002) J Mater Eng Perform 11(2):194
5. Wen S, Chung DDL (2001) Cem Concr Res 31(2):297
6. Wen S, Chung DDL (2000) Cem Concr Res 30(8):1289
7. Fu X, Lu W, Chung DDL (1998) Carbon 36(9):1337
8. Fu X, Chung DDL (1997) Cem Concr Res 27(9):1313
9. Chen P-W, Chung DDL (1993) Smart Mater Struct 2:22
10. Wen S, Chung DDL (2001) Cem Concr Res 31(4):665
11. Wen S, Chung DDL (2005) ACI Mater J 102(4):244
12. Sun M, Mao Q, Li Z (1998) J Wuhan Univ Technol, Mater Sci Ed 13(3):58
13. Mao Q, Zhao B, Sheng D, Li Z (1996) J Wuhan Univ Technol 11(3):41
14. Reza F, Batson GB, Yamamuro JA, Lee JS (2003) J Mater Civil Eng 15(5):476
15. Wu Y, Bing C, Keru W (2003) Mechanics and Material Engineering for Science and Experiments 172
16. Yao W, Chen B, Wu K (2003) J Mater Sci Technol 19(3):239
17. Wen S, Chung DDL (2006) Carbon 44(8):1496
18. Bontea D-M, Chung DDL, Lee GC (2000) Cem Concr Res 30(4):651
19. Fu X, Chung DDL (1996) Cem Concr Res 26(1):15
20. Chung DDL (2003) Mater Sci Eng R 42(1):1
21. Wen S, Chung DDL Cem. Conc r. Res., in press
22. Fu X, Chung DDL (1995) Cem Concr Res 25(7):1391
23. Chung DDL (2005) J Mater Civil Eng 17(4):379
24. Wen S, Chung DDL (2006) J Mater Civil Eng 18(3):355
25. Bisschop J, Van Mier JGM (2002) Cem Concr Res 32:279
26. Fu X, Chung DDL (1998) ACI Mater J 95(6):725
27. Fu X, Chung DDL (1997) Compos Interface 4(4):197